Advances in Particle Swarm Optimization for Antenna Designs: Real-Number, Binary, Single-Objective and Multiobjective Implementations

Nanbo Jin, *Student Member, IEEE*, and Yahya Rahmat-Samii, *Fellow, IEEE*

***Abstract*—The particle swarm optimization (PSO) is a recently developed evolutionary algorithm (EA) based on the swarm behavior in the nature. This paper presents recent advances in applying a versatile PSO engine to real-number, binary, single-objective and multiobjective optimizations for antenna designs, with a randomized Newtonian mechanics model developed to describe the swarm behavior. The design of aperiodic (nonuniform and thinned) antenna arrays is presented as an example for the application of the PSO engine. In particular, in order to achieve an improved peak sidelobe level (SLL), element positions in a nonuniform array are optimized by real-number PSO (RPSO). On the other hand, in a thinned array, the ON/OFF state of each element is determined by binary PSO (BPSO). Optimizations for both nonuniform arrays and thinned arrays are also expanded to multiobjective cases. As a result, nondominated designs on the Pareto front enable one to achieve other design factors than the peak SLL. Optimized antenna arrays are compared with periodic arrays and previously presented aperiodic arrays. Selected designs fabricated and measured to validate the effectiveness of PSO in practical electromagnetic problems.**

***Index Terms*—Aperiodic antenna array, binary optimization, multiobjective, optimization methods, particle swarm optimization (PSO), real-number optimization, single-objective.**

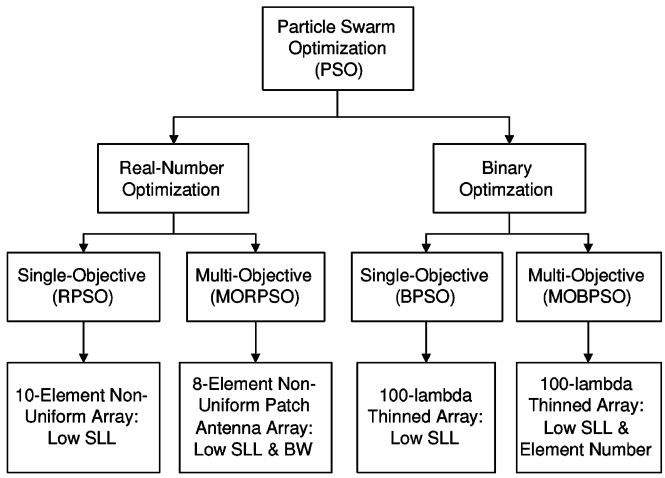

Fig. 1. Flowchart highlighting different optimization schemes addressed by the PSO engine and associated antenna array design examples presented in this paper.

I. Introduction

THE PSO algorithm was developed by Eberhart and Kennedy in 1995 [1] and was originated by imitating the behavior of a swarm of bees, a flock of birds or a school of fish during their food-searching activities [2]–[4]. Believed to be effective in multidimensional, linear and nonlinear problems, PSO was recently introduced into the antenna community by Robinson and Rahmat-Samii [5]. With various analytical and numerical tools available, PSO has been applied to different electromagnetic (EM) applications such as antenna pattern synthesis, reflector antenna shaping, patch antennas and EM absorber designs [6]–[12]. The parallel implementation of PSO enables fitness evaluations of all agents to be executed simultaneously, and substantially speeds up the optimization process [13].

Algorithm-wise, most of these applications can be categorized into *real-number* (or *continuous*) and *single-objective* optimizations. It means that the solution space is an infinite set, with each solution represented by a real-valued vector, and the relative quality of the solution is designated by only one weighted fitness function. However, there are many situations in which this standard version of PSO may not be sufficient. For instance, quite "typically in EM problems, the topology of a candidate design is discretized into “pixels” and could be represented more appropriately by a binary string instead of a real vector, which leads to a *binary*, or *combinatorial* optimization. In many other practical engineering applications, it is often desired to tradeoff the relative significance of more than one design factors, which results into *multiobjective* optimizations. As a robust algorithm to real-world problems, the PSO kernel is desired to be versatile enough to accommodate these different optimization schemes.

The goal of this paper is to present recent advances in applying PSO to real-number, binary, single-objective and multiobjective optimizations for antenna design applications. A flowchart of different PSO algorithms is shown in Fig. 1. As an example, these algorithms are applied to a class of antenna design problems—the design of aperiodic antenna arrays. The real-number PSO (RPSO) and binary PSO (BPSO) are applied to design *nonuniform* arrays and *thinned* arrays, respectively. The goal of the optimization is to achieve an improved peak sidelobe level (SLL) in the radiation pattern of the antenna array. To optimize other design factors such as the beamwidth

Manuscript received March 22, 2006; revised September 8, 2006.

The authors are with the Department of Electrical Engineering, University of California, Los Angeles, Los Angeles, CA 90095, USA (e-mail: jnnb@ee.ucla.edu; rahmat@ee.ucla.edu).

Color versions of one or more of the figures in this paper are available online at http://ieeexplore.ieee.org.

Digital Object Identifier 10.1109/TAP.2007.891552

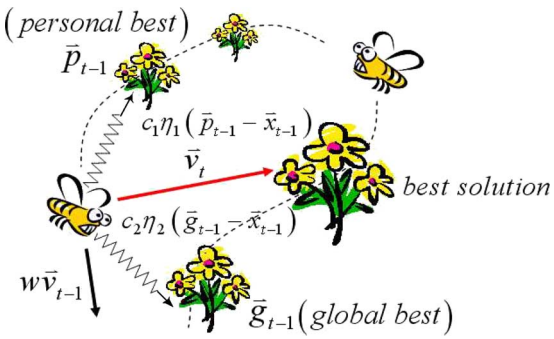

Fig. 2. Swarm of ambivalent bees (agents or particles) are flying in a field to find the location with the highest flower densities. The attractions from the personal best ($\vec{p}_{t-1}$) and the global best ($\vec{g}_{t-1}$) on each agent are modelled by Newtonian mechanics as two spring-like forces. c_1 and c_2 are Hooke's constants, multiplied by random numbers η_1 and η_2 with uniform distributions in (0,1) to inject the randomness. w is a time-varying inertial weight.

and the number of elements, multiobjective RPSO (MORPSO) and multiobjective BPSO (MOBPSO) are utilized in the design process, and the best strategy to tradeoff multiple factors is provided. Besides the analytical and numerical scrutiny, some optimized antenna arrays are selected, fabricated and measured to validate the effectiveness of the algorithm in practical designs.

Starting from basic Newtonian mechanics, Section II provides a conceptual overview of different optimization schemes addressed by the PSO engine. Section III presents the application of the PSO engine in four representative examples, along with measurement results of selected designs. The paper is summarized in Section IV.

II. The PSO Engine: A Randomized Newtonian Mechanics Model

A. Real-Number PSO (RPSO)

Fig. 2 depicts a swarm of ambivalent bees (designated as agents or particles) flying in a field (a solution space). The goal of each agent in the swarm is to find a location with the highest flower density. Assume the solution space is N-dimensional and real-valued, each location in the space, $\vec{x}$, is an N-dimensional real vector and is mapped into a candidate design with N unknowns. The flower density corresponds to the performance of the design which is represented by a fitness function. In this paper it is set as a default that a better performance leads to a smaller fitness value, and the optimizer is therefore a minimizer.

For each agent with a mass m, its time-varying position and velocity can be expressed by

$$\frac{d\vec{x}}{dt}=\vec{v};\quad \frac{d\vec{v}}{dt}=\vec{a}=\frac{\vec{F}}{m} \tag{1}$$

according to Newton's second law. Here, $\vec{F}$ denotes the force on the agent and $\vec{a}$ is the acceleration. $\vec{v}$ is an N-dimensional real vector that represents the velocity. In order to formulate an iterative process, we apply backward and forward differentiations to (1)

$$\frac{\vec{x}_t-\vec{x}_{t-1}}{\Delta t}=\vec{v}_t\Rightarrow\vec{x}_t=\vec{x}_{t-1}+\vec{v}_t\Delta t \tag{2}$$

$$\frac{\vec{v}_t-\vec{v}_{t-1}}{\Delta t}=\frac{\vec{F}_{t-1}}{m}\Rightarrow\vec{v}_t=\vec{v}_{t-1}+\frac{\vec{F}_{t-1}}{m}\Delta t. \tag{3}$$

If we further assume the mass of the agent, m, and the time step, Δt, are both unities, (2) and (3) reduce into

$$\vec{x}_t=\vec{x}_{t-1}+\vec{v}_t \tag{4}$$

$$\vec{v}_t=\vec{v}_{t-1}+\vec{F}_{t-1}. \tag{5}$$

Now the only unknown needs to be modelled in the iterative process is the force at the $(t-1)$th iteration, $\vec{F}_{t-1}$. An important feature underlying in the swarm behavior is that, each agent remembers the location that has the best fitness value on its own trajectory, which is defined as the *personal best* ($\vec{p}$). The best location found by the entire swarm, called the *global best* ($\vec{g}$), is also broadcasted to all agents to adjust their trajectories. Different cognitive and social influences on each agent can be modelled by applying different neighborhood topologies as detailed in [14] and [15]. In this paper, the influences from each agent's personal best and global best are modelled by two spring-like attractions, and $\vec{F}_{t-1}$ is expressed by

$$\vec{F}_{t-1}=c_1(\vec{p}_{t-1}-\vec{x}_{t-1})+c_2(\vec{g}_{t-1}-\vec{x}_{t-1}) \tag{6}$$

where c_1 and c_2 are Hooke's constants of two springs (see Fig. 2). Typically c_1 equals to c_2 in order to balance the cognitive part and the social part.

The behavior of the entire swarm can be expressed by writing the equations above in a matrix form. Let us assume an M-agent swarm in an N-dimensional solution space. Vectors $\vec{x}$'s, $\vec{v}$'s, $\vec{p}$'s and $\vec{g}$'s are stored in four $M\times N$ matrices $\mathbf{X}$, $\mathbf{V}$, $\mathbf{P}$ and $\mathbf{G}$, respectively. Equations (4)–(6) lead to matrix equations

$$\mathbf{X}_t=\mathbf{X}_{t-1}+\mathbf{V}_t \tag{7}$$

and

$$\mathbf{V}_t=\mathbf{V}_{t-1}+c_1(\mathbf{P}_{t-1}-\mathbf{X}_{t-1})+c_2(\mathbf{G}_{t-1}-\mathbf{X}_{t-1}). \tag{8}$$

To inject the randomness into the swarm behavior, Hooke's constants c_1 and c_2 are multiplied by random coefficients η_1 and η_2, respectively. In each dimension, both η_1 and η_2 have a uniform distribution in (0, 1), with $c_1=c_2=2.0$ suggested by [16] for the sake of convergence. To further accelerates the convergence, a time-varying *inertial weight*, w, is utilized and varies from 0.9 at the beginning to 0.4 toward the end of the optimization [17]. The velocity update in RPSO has a final form of

$$\mathbf{V}_t=w\mathbf{V}_{t-1}+c_1\eta_1(\mathbf{P}_{t-1}-\mathbf{X}_{t-1})+c_2\eta_2(\mathbf{G}_{t-1}-\mathbf{X}_{t-1}) \tag{9}$$

which is also depicted by Fig. 2.

To deal with agents flying out of the solution space is a unique problem in RPSO. A limitation in the maximum velocity, $V_{\max}$, can be imposed to prevent an agent from flying out of the physically meaningful solution space too often [16]. Its value is suggested to be equal to the dynamic range in each dimension of the agent. For instance, if a variable is allowed to be optimized within (a,b), the maximum velocity in this dimension is $|a-b|$ in both directions. However, this limitation does not always constrain the agent in the solution space. In [5], three basic

boundary handling techniques, the *absorbing* wall, the *reflecting* wall, and the *invisible* wall, are illustrated and compared. A hybrid "damping" boundary condition is also proposed recently [18] by applying some beneficial features of both absorbing and reflecting walls. In our RPSO algorithm, the invisible boundary condition is used due to its distinct advantage in reducing the computational cost.

B. Binary PSO (BPSO)

Now let us consider the velocity update in (8) in an N-dimensional binary solution space. At the $(t-1)$th iteration, the position of the mth agent can be expressed by an N-bit binary string

$$\{x_{mn,t-1}\} = \{x_{m1,t-1}, x_{m2,t-1}, \cdots, x_{mN,t-1}\} \qquad x_{mn,t-1} \in \{0,1\}. \quad (10)$$

Since each bit $x_{mn,t-1}$ is binary-valued, the Hamming distance between the agent's current position and its personal best (or its global best) has only three possible values

$$p_{mn,t-1} - x_{mn,t-1} = \begin{cases} 1; & p_{mn,t-1} = 1, \quad x_{mn,t-1} = 0 \\ 0; & p_{mn,t-1} = x_{mn,t-1} = 0 \\ & \quad or \\ -1. & p_{mn,t-1} = x_{mn,t-1} = 1 \\ & p_{mn,t-1} = 0, \quad x_{mn,t-1} = 1. \end{cases} \quad (11)$$

Multiplied by randomized Hooke's constants $(c_1\eta_1, c_2\eta_2)$ and added by the momentum part $v_{mn,t-1}$, the velocity $v_{mn,t}$ is still a real number in $[-V_{\max}, V_{\max}]$. Since $x_{mn,t}$ also has to be binary-valued, the agent's position must be updated in an alternative manner to that in (7).

The solution to this dilemma is addressed by Kennedy and Eberhart by investigating the meaning of the velocity in a binary space [19]. In binary PSO (BPSO), $v_{mn,t}$ is related to the possibility that $x_{mn,t}$ takes a value of 1 or 0. It is implemented by defining an intermediate variable $S(v_{mn,t})$ via the *sigmoid limiting transformation*

$$S(v_{mn,t}) = \frac{1}{1+e^{-v_{mn,t}}}. \quad (12)$$

Fig. 3 plots the range of $S(v_{mn,t})$ within its domain of $[-V_{\max}, V_{\max}]$. It is a monotonically increasing function with

$$S(v_{mn,t}) = \begin{cases} \frac{1}{1+e^{V_{\max}}} \to 0, & v_{mn,t} = -V_{\max} \to -\infty \\ \frac{1}{2}, & v_{mn,t} = 0 \\ \frac{1}{1+e^{-V_{\max}}} \to 1. & v_{mn,t} = V_{\max} \to \infty. \end{cases} \quad (13)$$

The sigmoid limiting transformation $S(x)$ maps its domain of $[-V_{\max}, V_{\max}]$ into the range of $[1/(1+e^{V_{\max}}), 1/(1+e^{-V_{\max}})]$, which is a subset of (0, 1). The value of $S(v_{mn,t})$ can be therefore interpreted as a probability threshold. A random number with a uniform distribution in (0, 1), $r_{mn,t}$, is then generated and compared to $S(v_{mn,t})$. The nth bit of the mth agent, $x_{mn,t}$, is updated by

$$x_{mn,t} = \begin{cases} 1, & r_{mn,t} < S(v_{mn,t}) \\ 0, & r_{mn,t} \geq S(v_{mn,t}). \end{cases} \quad (14)$$

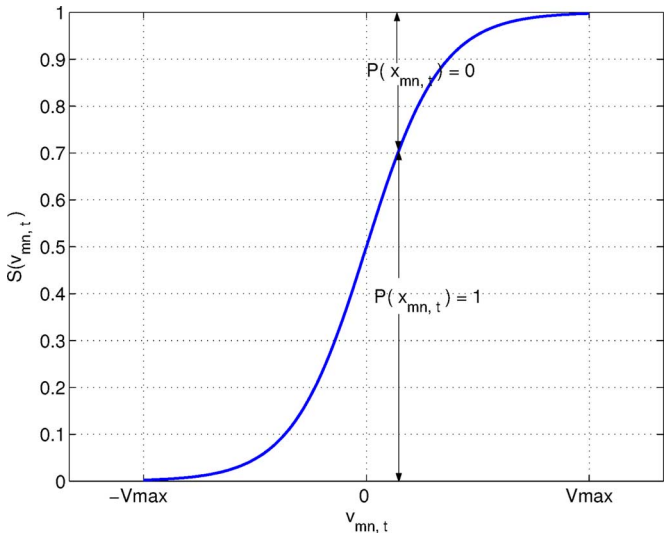

Fig. 3. Sigmoid limiting transformation over $[-V_{\max}, V_{\max}]$. It is a monotonically increasing function and represents the probability that a bit takes a value of 1 or 0.

The probability that the nth bit equals to 1 is

$$P(x_{mn,t} = 1) = S(v_{mn,t}) \quad (15)$$

and the probability that it equals to 0 is

$$P(x_{mn,t} = 0) = 1 - S(v_{mn,t}) = S(-v_{mn,t}). \quad (16)$$

Equations (12) and (14) indicates that a bit will be flipped with a greater probability, if it is different from the associated bit in the personal best or the global best. For instance, for the mth agent at the $(t-1)$th iteration, assume its nth bit is 0, while the nth bit of its personal best and global best are both 1. Its velocity at the tth iteration can be calculated by

$$\begin{aligned} v_{mn,t} &= v_{mn,t-1} + c_1\eta_1(p_{mn,t-1} - x_{mn,t-1}) \\ &\quad + c_2\eta_2(g_{mn,t-1} - x_{mn,t-1}) \\ &= v_{mn,t-1} + c_1\eta_1(1-0) + c_2\eta_2(1-0) \\ &= v_{mn,t-1} + c_1\eta_1 + c_2\eta_2 > v_{mn,t-1}. \end{aligned} \quad (17)$$

Since $S(x)$ is monotonically increasing, we have

$$S(v_{mn,t}) > S(v_{mn,t-1}). \quad (18)$$

It means that the nth bit tends to be 1 with a greater probability of $S(v_{mn,t})$, and the probability that the bit remains 0 is reduced by $S(v_{mn,t}) - S(v_{mn,t-1})$. If the bit is not flipped into 1 at the tth iteration, the velocity increases again at the $(t+1)$th iteration, along with a greater probability of $S(v_{mn,t+1})$ to flip the bit. Ultimately, with a limited velocity of $V_{\max}$, the probability of the nth bit to be flipped into 1 is

$$P(x_{mn,t} = 1) = \frac{1}{1+e^{-V_{\max}}} \to 1 \quad (19)$$

and the probability that it remains 0 is

$$P(x_{mn,t}=0)=1-P(x_{mn,t}=1)=\frac{1}{1+e^{V_{\max}}}\to 0. \quad (20)$$

In [19], a typical value of $V_{\max}=6.0$ is suggested, which corresponds to a maximum probability of 0.9975 that a bit is flipped into 1, and a minimum probability of 0.0025 that the bit remains 0. It is also noteworthy that the time-varying inertial weight in (9) does not improve the convergence of BPSO and a constant weight of 1.0 is suggested. No boundary handling techniques need to be specified in BPSO, since $x_{mn,t}$ is always a binary-valued quantity located in the solution space. The BPSO algorithm is validated using the standard testbed proposed in [20], which consists of five testing functions. In each test, a 10-agent swarm is observed to converge to the global optimum of 0 within 200 iterations.

C. Multiobjective PSO (MOPSO): The Notion of Pareto Front

Multiobjective optimizations arise from the need for a strategy to address multiple design factors in practical engineering problems. Assume the K factors considered in a design are represented by K fitness functions $f_i(\vec{x})$'s ($i=1,2,\ldots,K$ and $\vec{x}$ is a candidate design). Intuitively, these factors can be weighted and summed up to formulate a single-objective optimization

$$f(\vec{x})=\sum_{i=1}^{K} w_i f_i(\vec{x}) \quad (21)$$

and this method is called the conventional weighted aggregation (CWA). However, determining the best tradeoff between all factors requires understanding of the relative importance of each factor to the others. Although a simple method, CWA often requires an extensive tuning of weighting coefficients w_i's, particularly for problems where objectives are unrelated.

With multiple design goals in mind, the challenge of applying the swarm behavior is to determine the personal best and the global best of each agent. Parsopoulos and Vrahatis proposed the vector-evaluated PSO (VEPSO) [21], which utilizes a separate swarm for each design goal and each swarm has its own global best. After each iteration, the global bests of all swarms are exchanged. However, if there are more than two swarms operating in the solution space, it is not obvious how the global bests should be shared. On the other hand, the directed MOPSO (d-MOPSO) proposed by Fieldsend and Singh [22] is applied in our PSO engine due to its capability to handle more than two objectives.

The d-MOPSO is developed based on the concept of *Pareto dominance* [23]. For arbitrary $\vec{x}_1$ and $\vec{x}_2$, $\vec{x}_1$ *dominates* $\vec{x}_2$ if and only if their fitness vectors satisfy $f_i(\vec{x}_1)\le f_i(\vec{x}_2)$ for all i's and there exists at least one i that $f_i(\vec{x}_1)<f_i(\vec{x}_2)$. The set of all nondominated solutions is called the *Pareto front*. In d-MOPSO, the algorithm uses as each agent's global best the nondominated solution that is closest to that agent. The personal best is selected as the first nondominated solution explored by the agent. During the optimization, nondominated solutions are dynamically updated and stored according to the algorithm proposed in [24]. It is also noticed that the concept of Pareto dominance has been applied by Weile *et al.* [25] in genetic algorithms

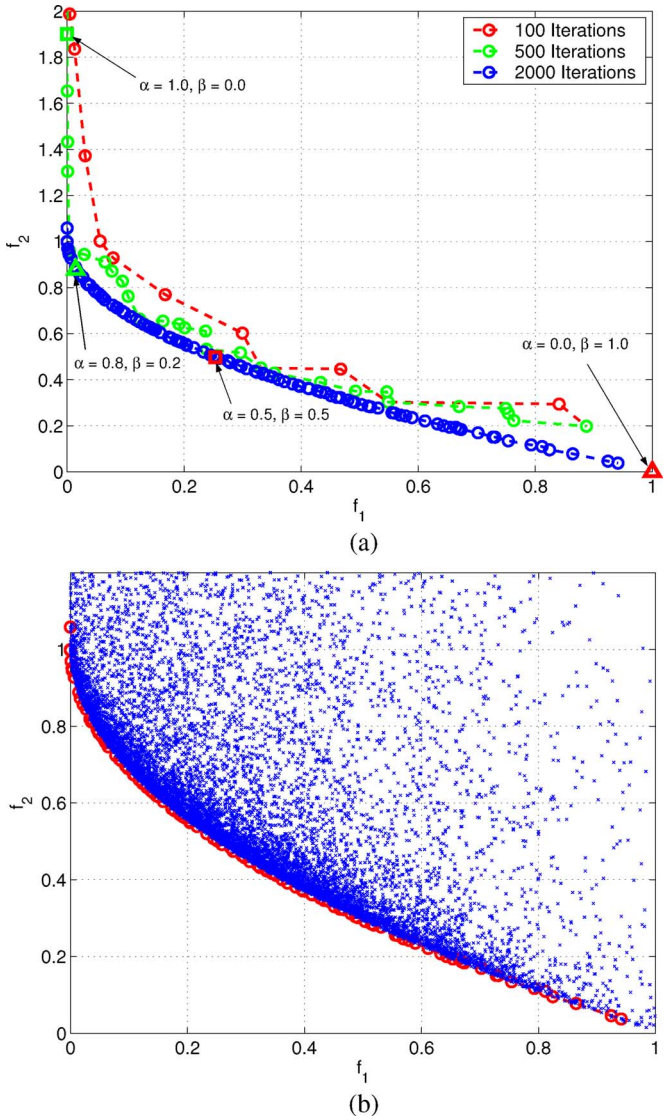

Fig. 4. (a) Pareto fronts of an MORPSO optimization at the 100th, the 500th and the 2000th iteration. Four CWA solutions are also plotted and compared to the Pareto fronts. (b) Fitness values of all positions visited by the swarm during the optimization. The swarm ultimately converges to the Pareto front.

(GA) for multiobjective optimizations. The navigation based on the Pareto front in d-MOPSO can be regarded as an alternative operator of the fitness sharing in Pareto GA.

Here, we use a representative testing problem proposed in [21] to pictorially illustrate the concept of a Pareto front and compare it to a single-objective optimization using CWA. In particular, two fitness functions are defined as

$$f_1=x_1 \quad f_2=g\times\left(1-\sqrt{f_1/g}\right)$$
$$g=1+\frac{9}{N-1}\sum_{i=2}^{N} x_i \quad (22)$$

to test a convex, nonuniform Pareto front. A 20-agent swarm is used in the optimization for 2000 iterations. Fig. 4(a) plots the Pareto fronts at the 100th, 500th, and 2000th iteration. It is observed that as the optimization proceeds, new Pareto fronts are explored and consist of more nondominated solutions.

The fitness function for CWA is defined as

$$f = \alpha f_1 + \beta f_2 \tag{23}$$

where f_1 and f_2 are defined in (22). The weighting coefficients, α and β, are two real numbers in [0, 1] and satisfy $\alpha + \beta = 1.0$. Four RPSO optimizations are executed using four possible weighting combinations: 1) $\alpha = 1.0$, $\beta = 0.0$; 2) $\alpha = 0.8$, $\beta = 0.2$; 3) $\alpha = 0.5, \beta = 0.5$; and 4) $\alpha = 0.0, \beta = 1.0$, with the emphasis on f_1 in a descending order. Each CWA optimization utilizes a 20-agent swarm for 2000 iterations. The fitness values of four RPSO solutions are also plotted in Fig. 4(a). Solutions 2, 3 and 4 are located on the Pareto front, whereas solution 1 ($\alpha = 1.0, \beta = 0.0$) is located far inside. It is clearly shown that CWA is able to obtain, at most, a solution on the Pareto front by extensively changing the weighting coefficients. The CWA solution may also be dominated by the Pareto front by using an inappropriate weighting combination, which is quite possible when there is no *a priori* knowledge of the solution space.

Fig. 4(b) plots fitness values of all positions visited by the swarm during the optimization. Ultimately the swarm converges to the Pareto front and no more nondominated solutions will be explored. The judgement of the convergence to an actual Pareto front is relatively easy in testing function cases, while it is not feasible in most engineering EM optimizations due to the complexity of the solution space. The nondominated solutions referred in this paper should be, more rigorously, regarded as quasi-Pareto optimal solutions. The paradigm of d-MOPSO applies to both RPSO and BPSO. In what follows, the associated real-number and binary algorithms will be referred as multiobjective RPSO (MORPSO) and multiobjective BPSO (MOBPSO), respectively.

III. PSO for Aperiodic Antenna Array Designs

Aperiodic antenna arrays have received great attention since 1960s with the advances in both radio astronomy and radar techniques [26]. To prevent grating lobes, an upper limit exists in the element spacing of conventional periodic arrays, which significantly increases the number of elements to achieve a desired narrow beamwidth. In contrast, nonuniform element spacings in an aperiodic array prohibits the periodicity in the array factor. With a given aperture size, the lack of periodicity enables a lower SLL and an inherently reduced number of elements. A second-order advantage of aperiodic arrays is that a low SLL design can be achieved by exciting all elements using a uniform amplitude [27]. In periodic arrays, the sidelobes are generally suppressed by tapering the amplitude, which results in the inefficiency in the attainable power and the difficulties in designing the feeding network.

In general, aperiodic arrays can be categorized into *nonuniform arrays* and *thinned arrays*, as shown in Fig. 5. In a nonuniform array, the number of elements is fixed and the element positions are arbitrarily changed to obtain a desired SLL; on the other hand, in a thinned array, a fraction of the elements in a periodic array are turned off to reduce the grating lobes resulted from the periodic grid. Past attempts to obtain lower peak SLLs of both types of arrays include analytical methods [28]–[30], numerical algorithms [31] and probabilistic approaches [32]–[35].

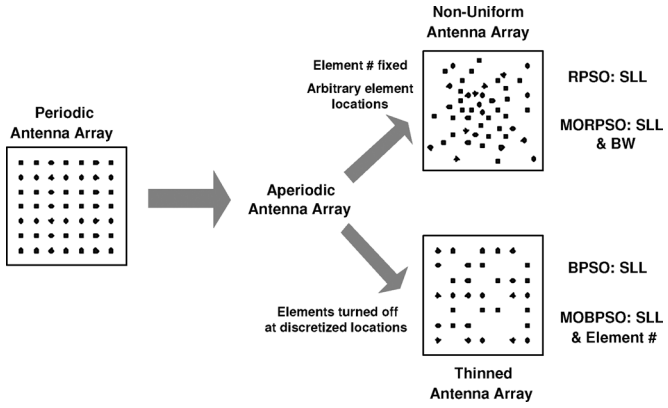

Fig. 5. Two scenarios for developing an aperiodic antenna array from a periodic antenna array: a nonuniform antenna array and a thinned antenna array. Different PSO algorithms are applied to different optimization goals.

However, since the peak SLL varies with the array configuration in an extremely nonlinear manner, a deterministic prediction of the peak SLL is not even possible. The limits given in [33] and [35] are both probabilistic-based. It is also proven in [34] that the lowest peak SLL of a thinned array can only be obtained via a brute-force search. Furthermore, the beamwidth of a nonuniform array and the element number of a thinned array are inherently determined when reducing the peak SLL. A strategy for a better design that trades-off the SLL and the beamwidth (or trades-off the SLL and the element number) has not been explicitly given.

For aperiodic antenna array designs, an attractive feature of PSO is that it accommodates both real-number (RPSO) and binary (BPSO) optimizations. This enables the PSO engine to be applied to design both nonuniform arrays and thinned arrays. In particular, RPSO determines element positions in a nonuniform array in terms of a real vector, and BPSO determines the on/off status of all elements in a thinned array represented by a binary string. The objective of both optimizations is to achieve the lowest peak SLL using a uniform amplitude. For multiobjective optimizations, MORPSO and MOBPSO algorithms handle other factors than the SLL, which allows the tradeoff between multiple criteria in designing aperiodic antenna arrays. All examples in this section are based on the design of linear arrays. The extension of the technique to two-dimensional and conformal aperiodic antenna arrays is rather straight-forward and is currently under investigation by the authors.

A. RPSO for Nonuniform Array Designs

First let us consider a 10-element nonuniform array of isotropic elements shown in Fig. 6(a). The array is assumed to be symmetric about the z-axis. The outermost elements are fixed at $x = \pm 2.25\lambda_0$, hence, there are four element locations need to be optimized by RPSO and the average element spacing is $d_{\text{avg}} = 0.5\lambda_0$. The problem is solved in a four-dimensional solution space defined as

$$\begin{aligned} &x_i \in (0, 2.25\lambda_0) \quad |x_i - x_j| > 0.25\lambda_0 \\ &\min\{x_i\} > 0.125\lambda_0. \quad i = 1, 2, 3, 4. \quad i \neq j. \end{aligned} \tag{24}$$

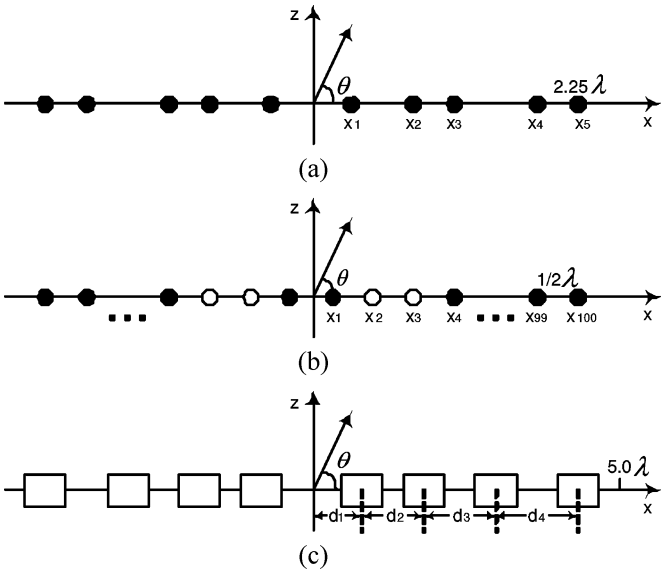

Fig. 6. Array configurations for different optimizations. (a) A 10-element, symmetric nonuniform array with the outermost elements fixed at $\pm 2.25\lambda_0$ for RPSO application, (b) a symmetric thinned array over an $100\lambda_0$ aperture discretized by $d = 0.5\lambda_0$ for BPSO and MOBPSO applications, (c) an 8-element nonuniform patch antenna array for MORPSO application. Notice the way in which the elevation angle θ is defined.

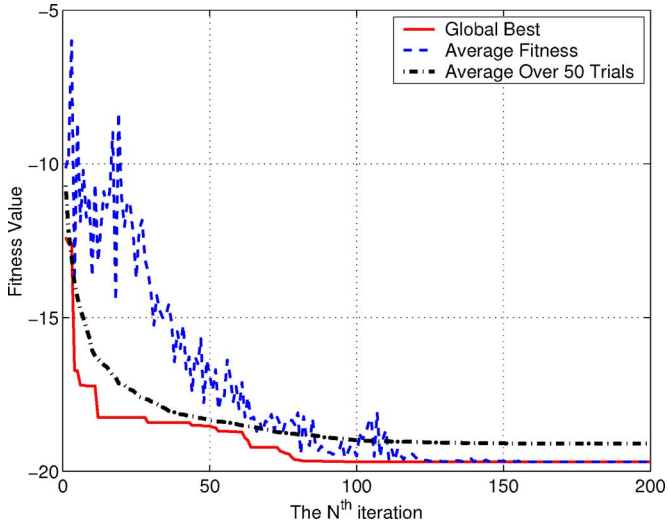

Fig. 7. Global best and average fitness of an RPSO optimization for a 10-element low SLL nonuniform array using the fitness function in (25). The optimization is executed for 50 independent trials, most of which are able to approach the global optimum.

Two adjacent elements are not allowed to get closer than $0.25\lambda_0$ while the solution space is sufficiently large to be explored. The antenna element in practice, for instance, a patch antenna, has a dimension around $0.5\lambda_0/\sqrt{\epsilon_r}$ if fabricated on a substrate with a dielectric constant ϵ_r. Another possibility in formulating the problem is to optimize the spacings $\{d_i\}$ between adjacent antenna elements, which will be illustrated later in an example of multiobjective optimization.

To achieve the lowest peak SLL, the optimization is modelled into a *minimax* problem using a fitness function of

$$f = \max\{20\log|AF(\theta)|\} \quad \text{in sidelobe region.} \tag{25}$$

where θ is defined in Fig. 6(a) and $AF(\theta)$ is the array factor calculated by

$$AF(\theta) = \sum_{i=1}^{4} \cos\left[2\pi x_i(\cos\theta - \cos\theta_s)\right] + \cos\left[2.25 \times 2\pi(\cos\theta - \cos\theta_s)\right]. \tag{26}$$

The last term is out of the summation and denotes the contribution of outermost elements fixed at $x = \pm 2.25\lambda_0$. θ_s is the beam-steering angle. We consider the broadside case first by taking $\theta_s = 90°$.

We have found that for an N-dimensional problem, the number of agents should be at least comparable to N. In this example the optimization is executed using a large number of 20 agents for 200 iterations to provide a better sampling of the solution space. Fig. 7 plots the global best and average fitness value at each iteration. The optimal design is observed at the 80th iteration with four inner elements located at

$$\{x_i\} = \{0.21\lambda_0, 0.60\lambda_0, 1.06\lambda_0, 1.59\lambda_0\}. \tag{27}$$

Fig. 7 also plots the average convergence over 50 independent trials. An average global best of -19.1 dB shows that most trials approach the global optimum. The radiation pattern of the optimal design is plotted in Fig. 8 with a peak SLL of -19.7 dB observed. As a comparison, a 10-element, $\lambda_0/2$-spaced periodic array has a peak SLL of -13 dB, which is dominated by its near-in sidelobes. Both arrays have approximately the same beamwidth due to the fixed aperture size. The directivities of the the periodic array and the nonuniform array are 10.0 dB and 9.9 dB, respectively, and the former can be easily predicted by $D = 2N(d/\lambda_0)$. It indicates that with the near-in sidelobes suppressed, the energy are spread to the far sidelobes of a nonuniform array. In other words, the peak SLL is reduced at the expense of higher rms sidelobes.

An interesting feature of the optimal nonuniform array is its resemblance to an equal-sidelobe design achieved by Dolph-Chebyshev method for periodic arrays [36]. This is resulted by using an appropriate fitness function in (25) to reduce the peak SLL, no matter where the peak sidelobe appears in the visible region. We also noticed that a fitness function with an integral form of

$$f = \sum_i \frac{1}{\Delta\theta_i} \int_{\theta_{li}}^{\theta_{ui}} |AF(\theta)|\,\mathrm{d}\theta \tag{28}$$

is recently proposed in [37], with $[\theta_{ui}, \theta_{ui}]$ representing the angular region where the sidelobes are suppressed. The peak SLL of the optimal design in [37] is only -17.4 dB, which is 2.3 dB higher than the example shown above. It is believed that the fitness function in (28) is utilized for the sake of suppressing the SLL as well as controlling the null position. In this particular problem of a low SLL design, however, it is a better option to formulate the optimization as a *minimax* problem and use (25) as the fitness function.

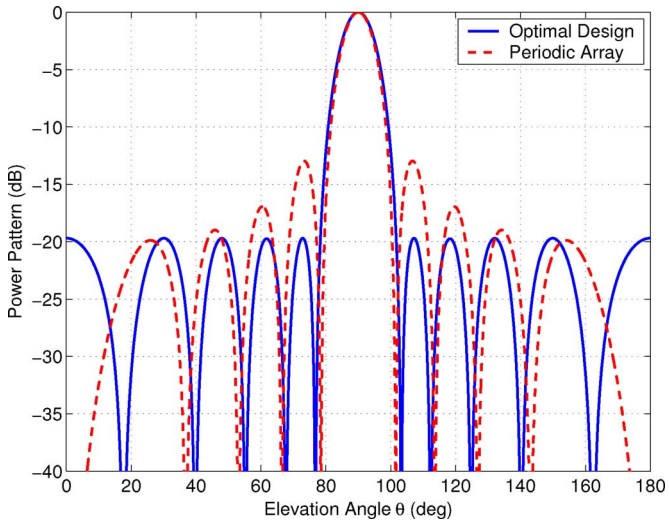

Fig. 8. Radiation patterns of the optimized 10-element nonuniform array and a 10-element periodic array with the same aperture size of $4.5\lambda_0$. The peak SLL is reduced from -13 dB to -19.7 dB.

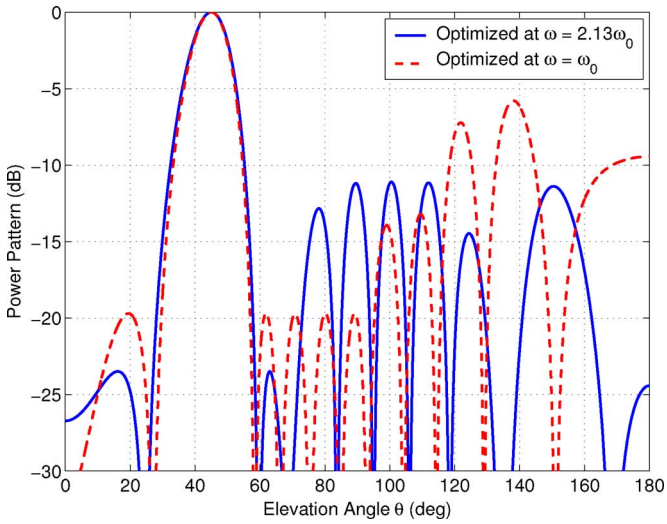

Fig. 9. Radiation patterns of the array optimized at $\omega = 2.13\omega_0$ and the optimal RPSO array shown by (27). Both arrays are operated at $\omega = 1.25\omega_0$ with the same beam steering angle of $\theta_s = 45^\circ$.

The method is also applicable to optimize a nonuniform array with a steered beam and a certain bandwidth. Assume a nonuniform array has a steered beam at θ_s and an upper bound operating angular frequency ω, the optimization of a low SLL array is equivalent to designing a broadside array at a nominal angular frequency of

$$\omega_n = \omega(1 + \cos\theta_s) \tag{29}$$

since both arrays have the same sidelobe feature in the visible region. For instance, for a 10-element array with a beam steered at 45° and a fractional bandwidth of 50% (with respect to a center frequency of ω_0), the nominal design frequency is calculated by

$$\omega_n = \left(1 + \frac{0.5}{2}\right)\omega_0(1 + \cos 45^\circ) = 2.13\omega_0. \tag{30}$$

Fig. 9 plots the radiation pattern of the optimal beam-steered array operated at $\omega = 1.25\omega_0$. Compared to the optimization of a broadside array, a deteriorated -11.1 dB peak SLL is observed due to the enlarged visible region. However, if the optimal array in (27) is operated under the same condition, the peak SLL is only -5.8 dB. The optimized -19.7 dB sidelobes in Fig. 8 only exist in the angular region close to the mainbeam. By realizing the similarity between these optimizations, the rest of the paper will focus on designing single-frequency, broadside arrays only.

B. BPSO for Thinned Array Designs

The design of a low SLL thinned array, on the other hand, is a binary optimization and is addressed by the BPSO algorithm. The optimization is usually based on a large aperture, in order to search a considerably large number of possible array configurations. Fig. 6(b) shows the configuration of a 100-λ_0 aperture discretized by a uniform grid of $\lambda_0/2$. The array is also assumed to be symmetric and only consists of isotropic elements. A similar fitness function to (25) is used to reduce the peak SLL, while the array factor is calculated in a slightly different manner. It is proposed in [38] that the initialization of candidate designs plays an important role to the convergence rate when optimizing thinned arrays. In this example, a random initialization with an equal 0/1 probability is applied to all elements to achieve a better sampling and a thorough exploration of the solution space.

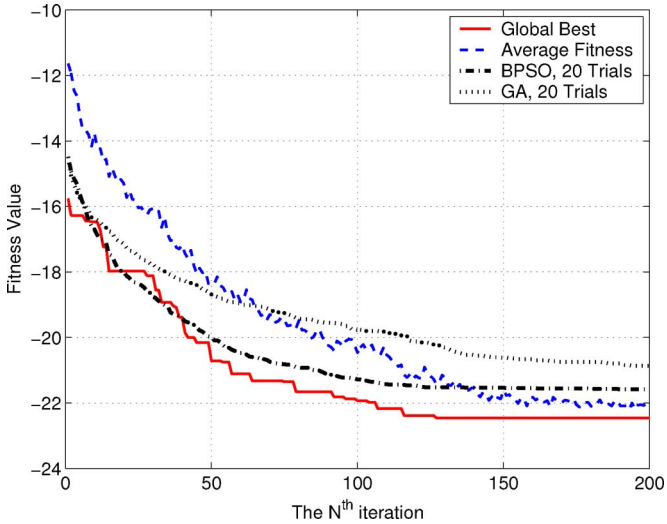

Fig. 10. Global best and average fitness of a BPSO optimization for a 100-λ_0 low SLL thinned array using the fitness function in (25). The convergence curves of BPSO and GA optimizations are also compared based on 20 independent trials for each method.

Fig. 10 shows the convergence of the optimization using 50 agents for 200 iterations. The optimal design appears at the 130th iteration and has a configuration of

$$\begin{aligned}\{x_i\} = \{&11111111111111111111111111\\ &11111111111111111111011111\\ &10110101110111101011001 01\\ &10101010000010111001100 11\}\end{aligned} \tag{31}$$

where "1" represents that an element is turned on and "0" represents a turned-off element. It is observed that there are more elements turned on near the center rather than near the edge.

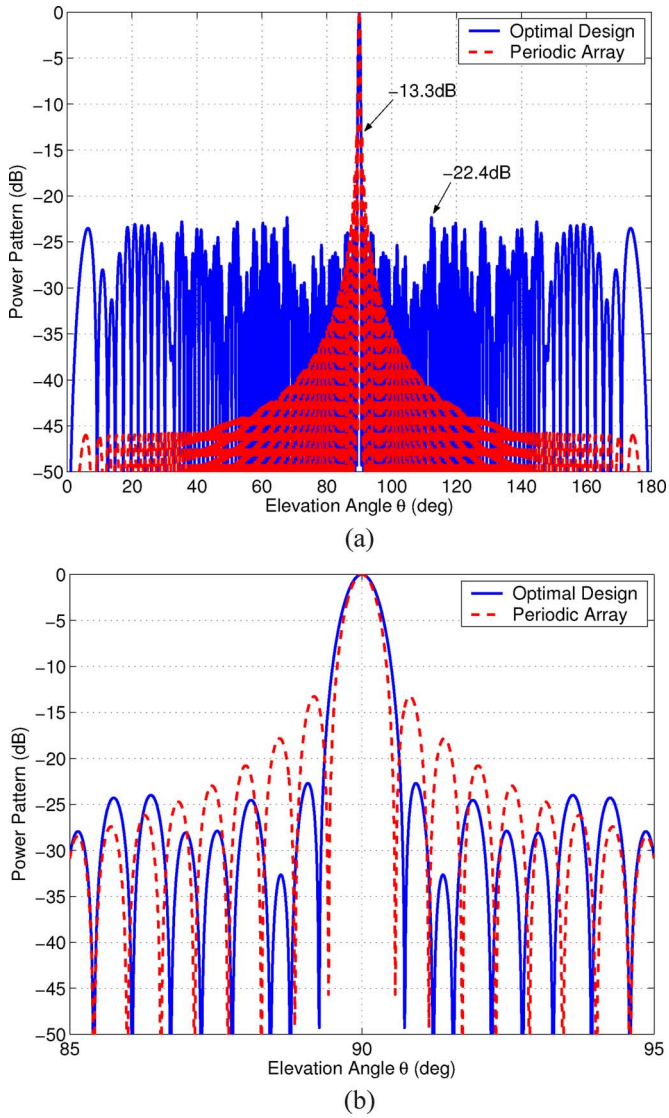

Fig. 11. (a) Radiation patterns of the optimized 100-λ_0 thinned array and a $\lambda_0/2$-spaced periodic array. The peak SLL is reduced from -13.3 to -22.4 dB. (b) Zoomed radiation patterns with elevation angles from 85° to 95°. The peak SLL of the periodic array is dominated by its -13.3 dB near-in sidelobe.

The aperture is filled by a factor of 77%. Fig. 11 plots radiation patterns of the optimal design and a periodic array with a uniform element spacing of $\lambda_0/2$ (a 100% filled aperture) in different ranges of elevation angles. Once again, the thinned array exhibits an equal-sidelobe feature, and the peak SLL is reduced from -13.3 to -22.4 dB. Note that the peak SLL of the periodic array is dominated by its first sidelobe which is very close to the main beam.

The same problem has been investigated by Haupt using the genetic algorithm (GA) [39] and an optimal design with a peak SLL of -22.1 dB is observed. As a further comparison, Fig. 10 shows convergence curves averaged over 20 independent trials for both BPSO and GA. The GA optimizations are executed using 50 chromosomes for 200 generations, with typical GA parameters of $p_{\text{cross}} = 0.7$ and $p_{\text{mut}} = 0.05$. It is observed that BPSO has a faster convergence and approaches a better fitness value in this particular problem, by selecting the same number of agents and chromosomes. A better GA design may be achieved by using more chromosomes and selecting other GA parameters.

C. MORPSO for Nonuniform Array Designs

In the single-objective RPSO example shown above, we achieve a low SLL nonuniform array by fixing the outermost element and varying inner elements. The optimized peak SLL can be therefore interpreted as the lowest peak SLL for this particular aperture size. In general, increasing the aperture size results in a narrower main beam but a deteriorated SLL. If the requirement in the SLL is relaxed for the beamwidth, multiobjective RPSO can be applied to provide the best strategy for trading-off the two design goals.

Let us consider an 8-element linear nonuniform array shown in Fig. 6(c). In this example we select an element number of eight for fabrication purposes, which will be shown in later sections. The optimization is aimed to investigate its peak SLL and beamwidth by varying the element spacings $\{d_i\}$ $(i = 1, 2, 3, 4)$, which are all real-numbers. The position of the outermost element is not fixed but is allowed to vary within $5.0\lambda_0$, which gives a maximum element spacing of $d_{\text{avg}} = 1.43\lambda_0$. The elements in this symmetric array are identical patch antennas on an $\epsilon_r = 2.2$ substrate. The dimension of each patch is $0.49\lambda_g \times 0.70\lambda_g$ $(0.33\lambda_0 \times 0.48\lambda_0)$, and all elements are coupled in the H-plane. To prevent adjacent elements from getting overlapped, the element spacings are subjected to

$$d_1 \in (0.24\lambda_0, 3.56\lambda_0) \qquad d_2, d_3, d_4 \in (0.48\lambda_0, 3.8\lambda_0)$$
$$\sum_{i=1}^{4} d_i \leq 5.0\lambda_0. \tag{32}$$

The lower bound of each variable is defined according to the width of a patch, and the upper bound is calculated by assuming other three patches are connected to each other. The boundary of the solution space represents a physically invalid configuration, however, it is observed that none of the optimized designs is located even near the boundary.

The peak SLL and the null-null beamwidth are represented by the following two fitness functions:

$$f_1 = \max\{20\log|AF(\theta) \times EF(\theta)|\}, \quad f_2 = 2\theta_n. \tag{33}$$

where $AF(\theta)$ and $EF(\theta)$ are the array factor and the element pattern, respectively. θ_n denotes the position of the first null. Generally, more iterations are required by a multiobjective optimization than a single-objective one, if the agent numbers in both optimizations are the same. This MORPSO optimization is executed for 4000 iterations using a 20-agent swarm. Fig. 12(a) plots the Pareto front. Each nondominated design located at (ξ, η) can be interpreted as, for any design that has a null-null beamwidth of η-degree, its peak SLL can not be lower than ξ-dB. The fitness values plotted in Fig. 12(b) show that the swarm is well converged to the Pareto front.

As a comparison, the beamwidth-SLL relationship of an 8-element periodic array is plotted in Fig. 12(a). This curve is completely dominated by the Pareto front, which indicates that an aperiodic array on the Pareto front always has a lower SLL than

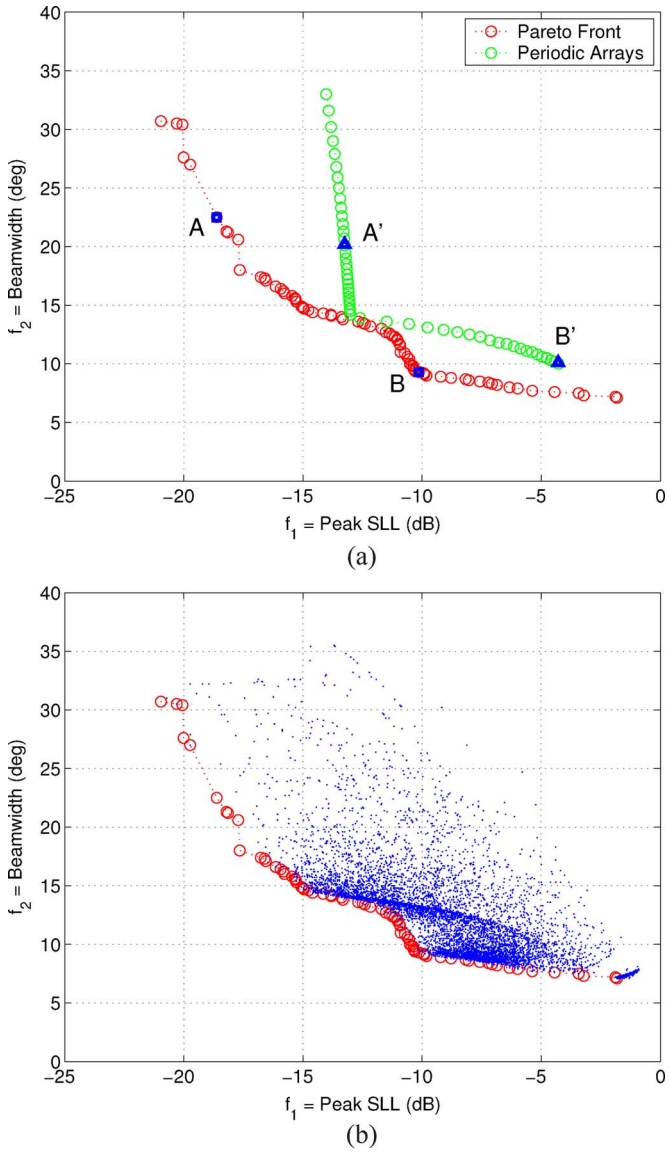

Fig. 12. (a) Pareto front of an MORPSO optimization for trading-off the peak SLL and the beamwidth of an 8-element nonuniform patch antenna array. The SLL-beamwidth relationship of periodic arrays is also plotted. (b) Fitness values of all positions visited by the swarm during the optimization.

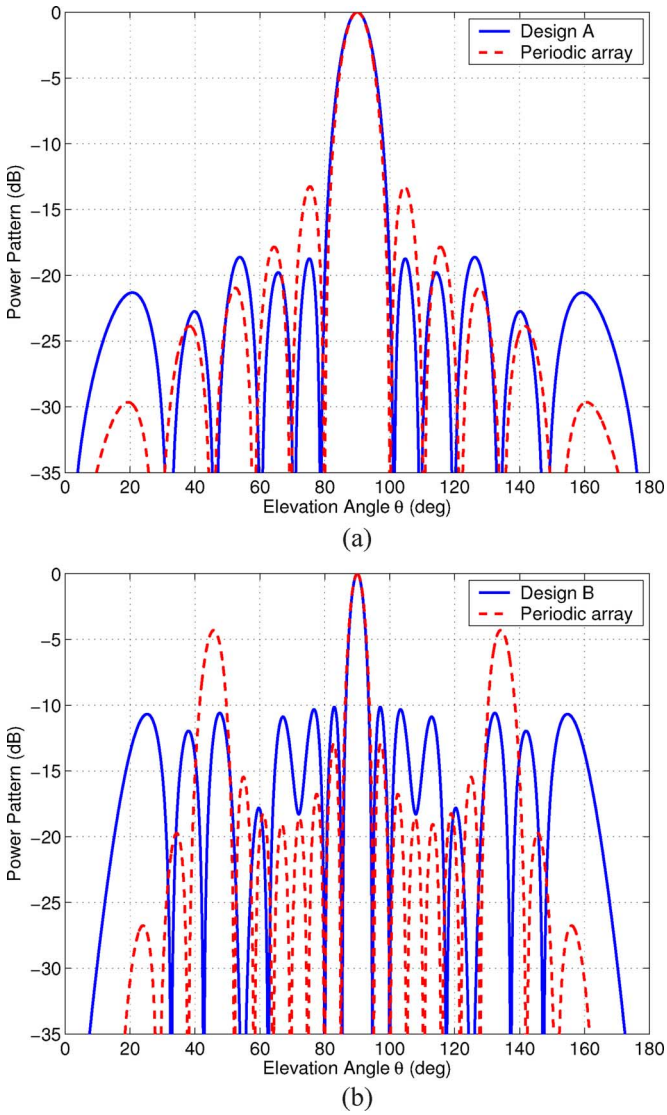

Fig. 13. Comparison of the radiation patterns of selected nonuniform arrays and periodic arrays with the same aperture sizes in Fig. 12(a). (a) Designs A and A'. (b) Designs B and B'.

a periodic array with the same beamwidth. For instance, designs A and B are two nondominated designs arbitrarily selected from the Pareto front with configurations of

$$\{d_{i,A}\} = \{0.32\lambda_0, 0.57\lambda_0, 0.72\lambda_0, 0.89\lambda_0\} \quad (34)$$

$$\{d_{i,B}\} = \{0.49\lambda_0, 2.17\lambda_0, 1.13\lambda_0, 1.21\lambda_0\} \quad (35)$$

and aperture sizes of $5\lambda_0$ and $10\lambda_0$, respectively. Compared to periodic arrays with the same aperture sizes, A' and B', the aperiodic arrays has similar beamwidths but significantly reduced peak SLLs. Their radiation patterns are plotted in Fig. 13. The peak SLL of design A' is reduced from -13.3 to -18.6 dB by A, with the directivities of A and A' 16.8 and 16.9 dB, respectively (notice that directional elements are used). The $10\lambda_0$-periodic array B' has a high SLL of -4.3 dB due to the strong grating lobes in the array factor, while design B has a much lower SLL of -10.1 dB by aperiodically arranging the elements and eliminating the grating lobes. The directivity is increased from 17.2 to 17.6 dB.

D. MOBPSO for Thinned Array Designs

The last example is to design an 100-λ_0 thinned array of isotropic elements, as shown in Fig. 6(b). In the array thinning process, turning off too many elements results in a high SLL. The MOBPSO algorithm is therefore applied to investigate the relationship between the peak SLL and the necessary element number to achieve a desired SLL. Two fitness functions of

$$f_1 = \max\{20\log|AF(\theta)|\}, \quad f_2 = 2\sum_{i=1}^{100} x_i \quad (36)$$

are used to evaluate the peak SLL and the element number, respectively. The optimization is executed using a 50-agent swarm for 2000 iterations. The Pareto front is plotted in Fig. 14 and

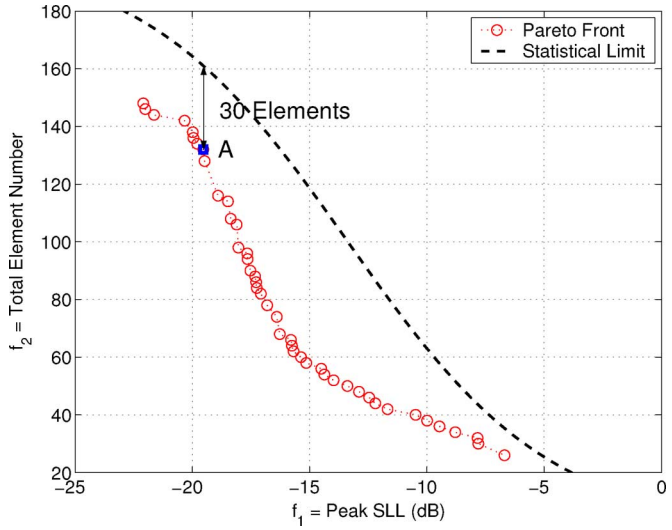

Fig. 14. Pareto front of an MOBPSO optimization for trading-off the peak SLL and the total turned-on element number of a 100-λ_0 thinned array. The SLL limit of statistical density tapering presented in [40] is plotted as a function of the total element number.

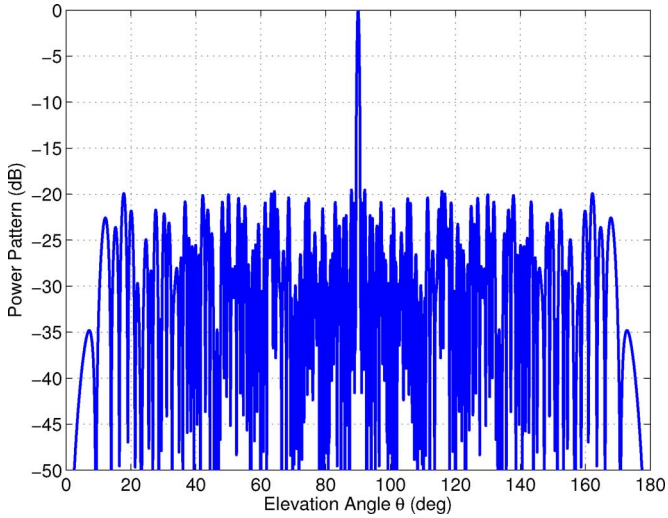

Fig. 15. Radiation pattern of a selected design A in Fig. 14. It has a peak SLL of -19.6 dB while 30 less elements than the array designed by statistical density tapering with the same peak SLL.

each nondominated design at (ξ, η) indicates that at least η elements are needed to achieve a peak SLL of ξ-dB.

A SLL limit is proposed in [40] for aperiodic arrays designed by statistical density tapering [32]. It states that p-percent of the sidelobes of a thinned array designed by statistical density tapering will be lower than a threshold value

$$r^2_{\text{peak}} = -r^2_{\text{avg}} \ln(1 - p^{2/N_{\text{total}}}) \tag{37}$$

where r^2_{avg} is the average SLL calculated by

$$r^2_{\text{avg}} = \frac{1}{N_{\text{on}}} - \frac{1}{N_{\text{total}}}. \tag{38}$$

In the above equations N_{on} and N_{total} are the number of turned ON elements and total elements, say, $N_{\text{on}} = f_2$ and $N_{\text{total}} = 200$. This limit is plotted in Fig. 14 as a function of N_{on} by taking a $p = 99$. The peak SLL can be approximately represented by r^2_{peak} since 99% sidelobes are lower than this threshold. It is observed that each nondominated design obtained by MOBPSO has fewer elements than the thinned array designed by statistical density tapering, with their peak SLLs the same.

For instance, design A is arbitrarily selected from the Pareto front with a configuration of

$$\begin{aligned}\{x_{i,A}\} = \{&11110111111111111111111011\\ &11111111111111001110011001\\ &11010010010011111101010110\\ &00010100110110001010110000\}.\end{aligned} \tag{39}$$

Its peak SLL is -19.6 dB, with 132 elements turned on in the entire aperture [66 elements in half of the aperture, as shown in (39)]. As a comparison, the statistical density tapering requires 162 elements to achieve the same peak SLL. Similar observation on the reduction of element number is presented in [39]. The radiation pattern of design A is plotted in Fig. 15. Compared to the optimal thinned array achieved by single-objective BPSO in (31), the latter has a 2.8 dB lower peak SLL while requires 22 more elements. Both arrays have similar beamwidths of 1.56° and 1.47°, respectively, and there are more turned-on elements concentrated near the center than at the edges in both array configurations. The rest of nondominated designs on the Pareto front, on the other hand, utilize different element numbers to tradeoff the peak SLL. However, since the beamwidth is not incorporated in the fitness function, different beamwidths are expected due to the varying aperture size.

E. Experimental Results for Selected Designs by MORPSO

The optimizations and analysis above are based on the fitness evaluations in (25), (33), and (36), without considering the mutual coupling, the edge effect, the feeding network and other factors when designing actual antenna arrays. To further validate the effectiveness of PSO technique in practical antenna array designs, we selected, fabricated and measured designs B and B' from the Pareto front in Fig. 12(a) achieved by MORPSO. Both arrays are fabricated on 0.508-mm thick RT/Duroid 5880 substrates and are designed to operate at 15 GHz. Each antenna element is matched to an 100 Ω transmission line. The feeding networks are carefully designed so that all antenna elements are excited by a uniform amplitude and a uniform phase. The total length of each array is 20.9 cm, with the centroids of two outermost elements separated by 20 cm ($10\lambda_0$ at 15 GHz). Fig. 16 shows both fabricated antenna prototypes.

Fig. 17(a) plots the S_{11} results with respect to 50 Ω measured at the input of feeding network. Both arrays have acceptable return losses of -16.2 and -17.7 dB at 15 GHz, respectively. The measured radiation patterns are shown in Fig. 17(b). It is observed that the -3.9 dB grating lobes of the periodic array are reduced to -9.6 dB, and the nonuniform array exhibits an approximate equal-sidelobe feature. Furthermore, the beamwidth, the number and the location of sidelobes of both arrays agree fairly well with Fig. 13(b). This is very interesting since the patterns in Fig. 13(b) are simply calculated by the product of the array factor and the element pattern. In these

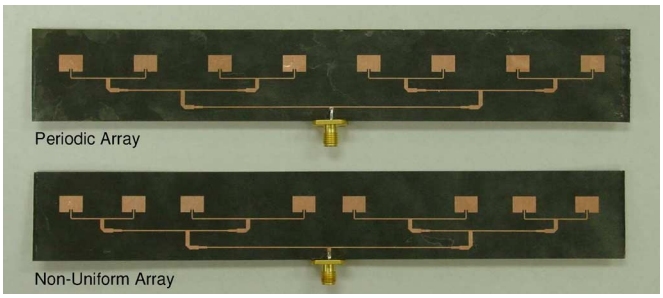

Fig. 16. Photograph of fabricated antenna arrays: A selected 8-element nonuniform array, design B in Fig. 12(a), and an 8-element periodic array with the same aperture size, design B' in Fig. 12(a).

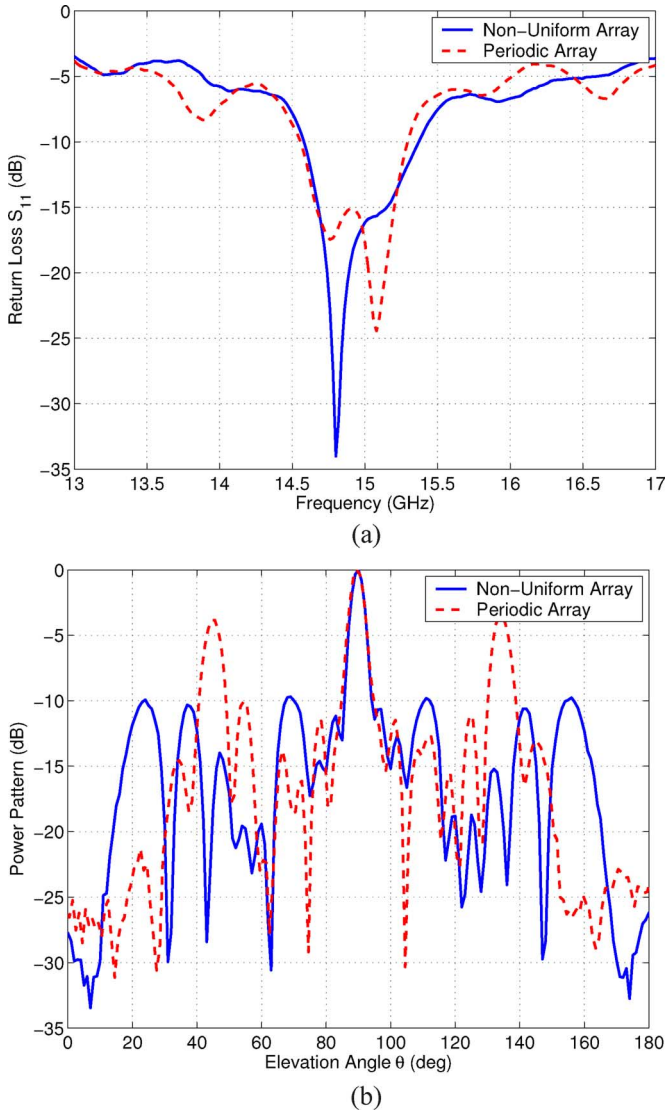

Fig. 17. (a) Measured return loss results. Both arrays have a return loss less than −15 dB at 15 GHz. (b) Measured radiation patterns at 15 GHz. The grating lobes of the periodic array are eliminated by the nonuniform array configuration.

broadside arrays, the mutual coupling is considerably small due to a large $d_{\text{avg}} = 1.43\lambda_0$, which makes the optimization result a good prediction for designing a low SLL array with a sparse configuration.

IV. Conclusion

This paper presents the full capability of a PSO engine developed at UCLA in real-number, binary, single-objective and multiobjective optimizations. A randomized Newtonian mechanics model is established to describe the swarm behavior applied by the algorithm. The PSO engine is utilized to design aperiodic antenna arrays as an example for its applications in engineering EM problems. Single-objective PSO algorithms (RPSO and BPSO) are used to optimize aperiodic antenna arrays with the lowest peak SLL for a uniform excitation. The candidate design can be either a nonuniform array or a thinned array. Multiobjective implementations of the PSO algorithm (MORPSO and MOBPSO), on the other hand, handle other design criteria than the lowest peak SLL. Optimized aperiodic arrays are observed to have improved performance over periodic arrays and previously presented aperiodic arrays. Some selected designs were further fabricated and measured to validate the effectiveness of the PSO engine in solving practical problems.

References

[1] J. Kennedy and R. Eberhart, "Particle swarm optimization," in *Proc. IEEE Int. Conf. Neural Networks*, 1995, vol. 4, pp. 1942–1948.
[2] M. Clerc and J. Kennedy, "The particle swarm—explosion, stability and convergence in a multidimensional complex space," *IEEE Trans. Evol. Comput.*, vol. 6, no. 1, pp. 58–73, Feb. 2002.
[3] Y. Shi and R. Eberhart, "Empirical study of particle swarm optimization," in *Proc. Cong. Evol. Comput.*, 1999, vol. 3, pp. 1945–1950.
[4] R. Eberhart and Y. Shi, "Particle swarm optimization: developments, applications, and resources," in *Proc. Cong. Evol. Comput.*, 2001, vol. 1, pp. 81–86.
[5] J. Robinson and Y. Rahmat-Samii, "Particle swarm optimization in electromagnetics," *IEEE Trans. Antennas Propag.*, vol. 52, no. 2, pp. 397–407, Feb. 2004.
[6] D. Gies and Y. Rahmat-Samii, "Particle swarm optimization for reconfigurable phase-differentiated array design," *Microwave Opt. Technol. Lett.*, vol. 38, no. 3, pp. 172–175, Aug. 2003.
[7] D. Boeringer and D. Werner, "Particle swarm optimization versus genetic algorithms for phased array synthesis," *IEEE Trans. Antennas Propag.*, vol. 52, no. 3, pp. 771–779, Mar. 2004.
[8] D. Gies and Y. Rahmat-Samii, "Particle swarm optimization (PSO) for reflector antenna shaping," in *IEEE Antennas Propag. Soc. Int. Symp. Dig.*, Jun. 2004, vol. 3, pp. 2289–2293.
[9] W. Liu, "Design of multiband CPW-fed monopole antenna using a particle swarm optimization approach," *IEEE Trans. Antennas Propag.*, vol. 53, no. 10, pp. 3273–3279, Oct. 2005.
[10] S. Cui and D. Weile, "Application of parallel particle swarm optimization scheme to the design of electromagnetic absorbers," *IEEE Trans. Antennas Propag.*, vol. 53, no. 11, pp. 3616–3624, Nov. 2005.
[11] L. Matekovits, M. Mussetta, P. Pirinoli, S. Selleri, and R. Zich, "Improved PSO algorithms for electromagnetic optimization," in *IEEE Antennas Propag. Soc. Int. Symp. Dig.*, Jul. 2005, vol. 2A, pp. 33–36.
[12] S. Mikki and A. Kishk, "Investigation of the quantum particle swarm optimization technique for electromagnetic applications," in *IEEE Antennas Propag. Soc. Int. Symp. Dig.*, Jul. 2005, vol. 2A, pp. 45–48.
[13] N. Jin and Y. Rahmat-Samii, "Parallel particle swarm optimization and finite difference time-domain (PSO/FDTD) algorithm for multiband and wide-band patch antenna designs," *IEEE Trans. Antennas Propag.*, vol. 53, no. 11, pp. 3459–3468, Nov. 2005.
[14] J. Kennedy, "Small worlds and mega-minds: effects of neighborhood topology on particle swarm performance," in *Proc. Cong. Evol. Comput.*, 1999, vol. 3, pp. 1931–1938.
[15] R. Mendes, J. Kennedy, and J. Neves, "Watch thy neighbor or how the swarm can learn from its environment," in *Proc. IEEE Swarm Intell. Symp.*, 2003, pp. 88–94.
[16] R. Eberhart and Y. Shi, "Particle swarm optimization: developments, applications and resources," in *Proc. Cong. Evol. Comput.*, 2001, vol. 1, pp. 81–86.
[17] ——, "Evolving artificial neural networks," in *Proc. Int. Conf. Neural Networks and Brain*, 1998, pp. PL5–PL13.
[18] T. Huang and A. Mohan, "A hybrid boundary condition for robust particle swarm optimization," *IEEE Antennas Wireless Propagat. Lett.*, vol. 5, pp. 112–117, 2005.

[19] J. Kennedy and R. Eberhart, "A discrete binary version of the particle swarm algorithm," in *Proc. IEEE Int. Conf. Systems, Man, and Cybernetics*, Oct. 1997, vol. 5, pp. 4104–4108.
[20] Y. Liao and C. Sun, "An educational genetic algorithms learning tool," *IEEE Trans. Educ.*, vol. 44, no. 2, May 2001.
[21] K. Parsopoulos and M. Vrahatis, "Recent approaches to global optimization problems through particle swarm optimization," *Natural Computing*, vol. 1, pp. 235–306, 2002.
[22] J. Fieldsend and S. Singh, "A multi-objective algorithm based upon particle swarm optimization, an efficient data structure and turbulence," in *Proc. U.K. Workshop on Computational Intellegence*, 2002, pp. 37–44.
[23] D. Velduizen, J. Zydallis, and G. Lamont, "Considerations in engineering parallel multiobjective evolutionary optimizations," *IEEE Trans. Evol. Comput.*, vol. 7, no. 2, pp. 144–173, Apr. 2003.
[24] Y. Jin, M. Olhofer, and B. Sendhoff, "Dynamic weighted aggregation for evolutionary multiobjective optimization: Why does it work and how?," in *Conf. Genetic Evol. Comput.*, 2001.
[25] D. S. Weile and E. Michielssen, "Genetic algorithms: theory and advanced techniques," in *Electromagnetic Optimization by Genetic Algorithms*, Y. Rahmat-Samii and E. Michielssen, Eds. New York: Wiley, 1999.
[26] G. Swenson and Y. T. Lo, "The university of illinois radio telescope," *IEEE Trans. Antennas Propag.*, vol. 9, no. 1, pp. 9–16, Jan. 1961.
[27] Y. T. Lo, "Aperiodic arrays," in *Antenna Handbook*, Y. T. Lo and S. W. Lee, Eds. New York: Van Nostrand Reihold, 1988.
[28] H. Unz, "Linear arrays with arbitrarily distributed elements," *IEEE Trans. Antennas Propag.*, vol. 8, no. 2, pp. 222–223, Mar. 1960.
[29] A. Ishimaru, "Theory of unequally-spaced arrays," *IEEE Trans. Antennas Propag.*, vol. 10, no. 6, pp. 691–702, Nov. 1962.
[30] R. Harrington, "Side lobe reduction by nonuniform element spacing," *IEEE Trans. Antennas Propag.*, vol. 9, no. 2, pp. 187–192, Mar. 1961.
[31] M. Skolnik, G. Nemhauser, and J. Sherman, III, "Dynamic programming applied to unequally spaced arrays," *IEEE Trans. Antennas Propag.*, vol. 12, no. 1, pp. 35–43, Jan. 1964.
[32] M. Skolnik, J. Sherman, III, and F. Ogg, "Statistically designed density-tapered array," *IEEE Trans. Antennas Propag.*, vol. 12, no. 4, pp. 408–417, Jul. 1964.
[33] Y. T. Lo, "A mathematical theory of antenna arrays with randomly space elements," *IEEE Trans. Antennas Propag.*, vol. 12, no. 2, pp. 257–268, May 1964.
[34] Y. T. Lo and S. W. Lee, "A study of space-tapered arrays," *IEEE Trans. Antennas Propag.*, vol. 14, no. 1, pp. 22–30, Jan. 1966.
[35] B. Steinberg, "The peak sidelobe of the phased array having randomly located elements," *IEEE Trans. Antennas Propag.*, vol. 20, no. 2, pp. 129–136, Mar. 1972.
[36] R. S. Elliot, *Antenna Throry and Design*. Hoboken, New Jersey: Wiley., 2003.
[37] M. Khodier and C. Christodoulou, "Linear array geometry synthesis with minimum sidelobe level and null control using particle swarm optimization," *IEEE Trans. Antennas Propag.*, vol. 53, no. 8, pp. 2674–2679, Aug. 2005.
[38] K. Chellapilla, S. S. Rao, and A. Hoorfar, "Optimization of thinned phased arrays using evolutionary programming," in *Proc. The 7th Int. Conf. on Evolutionary Programming*, Mar. 1998, pp. 157–166.
[39] R. Haupt, "Thinned arrays using genetic algorithms," in *Electromagnetic Optimization by Genetic Algorithms*, Y. Rahmat-Samii and E. Michielssen, Eds. New York: Wiley, 1999.
[40] B. Steinberg, *Microwave Imaging With Large Antenna Arrays*. New York: Wiley, 1983.

Nanbo Jin (S'03) received the B.S. degree from Tsinghua University, Beijing, China, in 2003, and the M.S. degree from the University of California, Los Angeles (UCLA), in 2005, both in electrical engineering. He is currently working toward the Ph.D. degree in electrical engineering at the University of California, Los Angeles.

From 2001 to 2003, he was a Research Assistant in the State Key Laboratory of Microwave and Digital Communications, Tsinghua University. Since August 2003, he has been working as a Graduate Research Assistant in the UCLA Antenna Laboratory. His research interests include evolutionary optimization techniques, reconfigurable antennas, antenna arrays and periodic structures in electromagnetic applications.

Yahya Rahmat-Samii (S'73–M'75–SM'79–F'85) received the M.S. and Ph.D. degrees in electrical engineering from the University of Illinois, Urbana-Champaign.

He is a Distinguished Professor and past Chairman of the Electrical Engineering Department, University of California, Los Angeles (UCLA). He was a Senior Research Scientist with the National Aeronautics and Space Administration (NASA) Jet Propulsion Laboratory (JPL), California Institute of Technology prior to joining UCLA in 1989. In summer 1986, he was a Guest Professor with the Technical University of Denmark (TUD). He has also been a consultant to numerous aerospace and wireless companies. He has been Editor and Guest editor of numerous technical journals and books. He has authored and coauthored over 690 technical journal and conference papers and has written 25 book chapters. He is a coauthor of *Implanted Antennas in Medical Wireless Communications* (San Rafael, CA: Morgan & Claypool, 2006), *Electromagnetic Optimization by Genetic Algorithms* (New York: Wiley, 1999) and *Impedance Boundary Conditions in Electromagnetics* (New York: Taylor & Francis, 1995). He has received several patents. He has had pioneering research contributions in diverse areas of electromagnetics, antennas, measurement and diagnostics techniques, numerical and asymptotic methods, satellite and personal communications, human/antenna interactions, frequency selective surfaces, electromagnetic band-gap structures, applications of the genetic algorithms and particle swarm optimization.

Dr. Rahmat-Samii is a Fellow of the Institute of Advances in Engineering (IAE) and a member of Sigma Xi, Eta Kappa Nu, Commissions A, B, J, and K of the United States National Committee of The International Union of Radio Science (USNC/URSI), the Antenna Measurement Techniques Association (AMTA), and The Electromagnetics Academy (TEA). For his contributions, he has received numerous NASA and JPL Certificates of Recognition. In 1984, he received the Henry Booker Award from URSI, which is given triennially to the most outstanding young radio scientist in North America. In 1992 and 1995, he received the Best Application Paper Prize Award (Wheeler Award) for papers published in 1991 and 1993 IEEE TRANSACTIONS ON ANTENNAS AND PROPAGATION. In 1999, he received the University of Illinois ECE Distinguished Alumni Award. In 2000, he received the IEEE Third Millennium Medal and the AMTA Distinguished Achievement Award, in 2001. He received an Honorary Doctorate in physics from the University of Santiago de Compostela, Spain, in 2001, and also became a Foreign Member of the Royal Flemish Academy of Belgium for Science and the Arts that same year. In 2002, he received the Technical Excellence Award from JPL. He received the 2005 URSI Booker Gold Medal presented at the URSI General Assembly. He was Vice-President and President of the IEEE Antennas and Propagation Society, in 1994 and 1995, respectively. He was appointed an IEEE AP-S Distinguished Lecturer and presented lectures internationally. He was a member of the Strategic Planning and Review Committee (SPARC) of the IEEE. He was the IEEE AP-S Los Angeles Chapter Chairman (1987–1989); his chapter won best chapter awards in two consecutive years. He is listed in *Who's Who in America*, *Who's Who in Frontiers of Science and Technology*, and *Who's Who in Engineering*. He is the designer of the IEEE Antennas and Propagation Society (IEEE AP-S) logo displayed on all IEEE AP-S publications. He has been the plenary and millennium session speaker at numerous national and international symposia. He has been the organizer and presenter of many successful short courses worldwide. He was a Director and Vice President of AMTA for three years. He has been Chairman and Co-chairman of several national and international symposia. He was a member of the University of California at Los Angeles (UCLA) Graduate council for three years.